JOURNAL OF GEOPHYSICAL RESEARCH, VOL. 115, C06016, doi:10.1029/2009JC005483, 2010

Comparisons of upwelling and relaxation events in the Monterey Bay area

Igor Shulman,[1] Stephanie Anderson,[1] Clark Rowley,[1] Sergio DeRada,[1] James Doyle,[2] and Steven Ramp[3]

Received 4 May 2009; revised 22 January 2010; accepted 4 February 2010; published 22 June 2010.

[1] Observations show significant differences in circulation patterns of upwelling and relaxation events that occurred in the Monterey Bay during two Autonomous Ocean Sampling Network field experiments in August 2003 and 2006. During the 2003 experiment, circulation exhibited more typical patterns associated with upwelling/relaxation: the development of the southward flowing jet and pair of cyclonic (inside of the bay) and anticyclonic (outside of the bay) circulations during upwelling and the development of the northward flow along the coast during relaxation of winds. During the upwelling event of 2006, the southward flow was weaker and shallower than in 2003. The second relaxation event of 2006 was significantly different from the first relaxation event of 2006 and the relaxation event of 2003: a southward flow was present along the entrance to the bay and this southward flow penetrated into the subsurface up to around 50 m at the mooring location. Two reasons for the observed differences in upwelling and relaxation events of 2003 and 2006 are identified in the paper: weaker winds in August 2006 than in August 2003 and strong positive sea surface height anomalies propagating poleward along the coast during 2006. The 2003 field program included an extensive sampling of the bay and surrounding areas with a fleet of underwater gliders, while during 2006 program, the extensive sampling was conducted in the area of upwelling center to the north of the Monterey Bay. During the 2003 field program, the Monterey Bay model was able to reproduce observed surface and subsurface features with assimilation of glider observations. However, during the 2006 field program, the assimilation of glider data from the upwelling center to the north of the Monterey Bay had minimal impact on model simulations of observed features to the south of the upwelling center.

Citation: Shulman, I., S. Anderson, C. Rowley, S. DeRada, J. Doyle, and S. Ramp (2010), Comparisons of upwelling and relaxation events in the Monterey Bay area, *J. Geophys. Res.*, *115*, C06016, doi:10.1029/2009JC005483.

1. Introduction

[2] Upwelling and relaxation events on the West Coast of the United States have been the subject of many studies [e.g., *Beardsley and Lentz*, 1987; *Winant et al.*, 1987; *Ramp et al.*, 2005]. During the Coastal Ocean Dynamics Experiment (CODE) of Pt Arena, California [*Beardsley and Lentz*, 1987] a variety of observations have shown the complex three-dimensional structure of the shelf response with the development of an equatorward near-surface jet during upwelling events, and a poleward flow near the coast during relaxation events. In the Monterey Bay area, the development of a southward flowing jet was also often observed during upwelling events [*Rosenfeld et al.* 1994; *Ramp et al.*, 2005, 2009]. This jet separates a pair of cyclonic (inside of the bay) and anticyclonic (outside of the bay) circulations. During relaxation events, the anticyclonic California Current meander moves onshore, and the currents on the continental shelf become poleward (see, for example, *Rosenfeld et al.* [1994] and *Ramp et al.* [2005] for more details).

[3] Multi-institution, multidisciplinary Autonomous Ocean Sampling Network (AOSN) field experiments were conducted in the Monterey Bay, California, during August and September 2003 and 2006. The objective of this network was to create a cohesive integration of real-time data collection, data assimilation, and modeling and prediction efforts across disciplinary lines (http://www.mbari.org/aosn/). The objectives of the 2003 experiment (called ASON-II [*Ramp et al.*, 2009]), included the application of new tools, technologies, and analysis techniques to adaptively sample the coastal ocean, and the development of accurate forecasts of the bay-scale patterns of physical and biological fields, including bioluminescence [*Moline et al.*, 2009; *Shulman et*

[1]Oceanography Division, Naval Research Laboratory, Stennis Space Center, Mississippi, USA.
[2]Marine Meteorology Division, Naval Research Laboratory, Monterey, California, USA.
[3]Monterey Bay Aquarium Research Institute, Moss Landing, California, USA.

0148-0227/10/2009JC005483

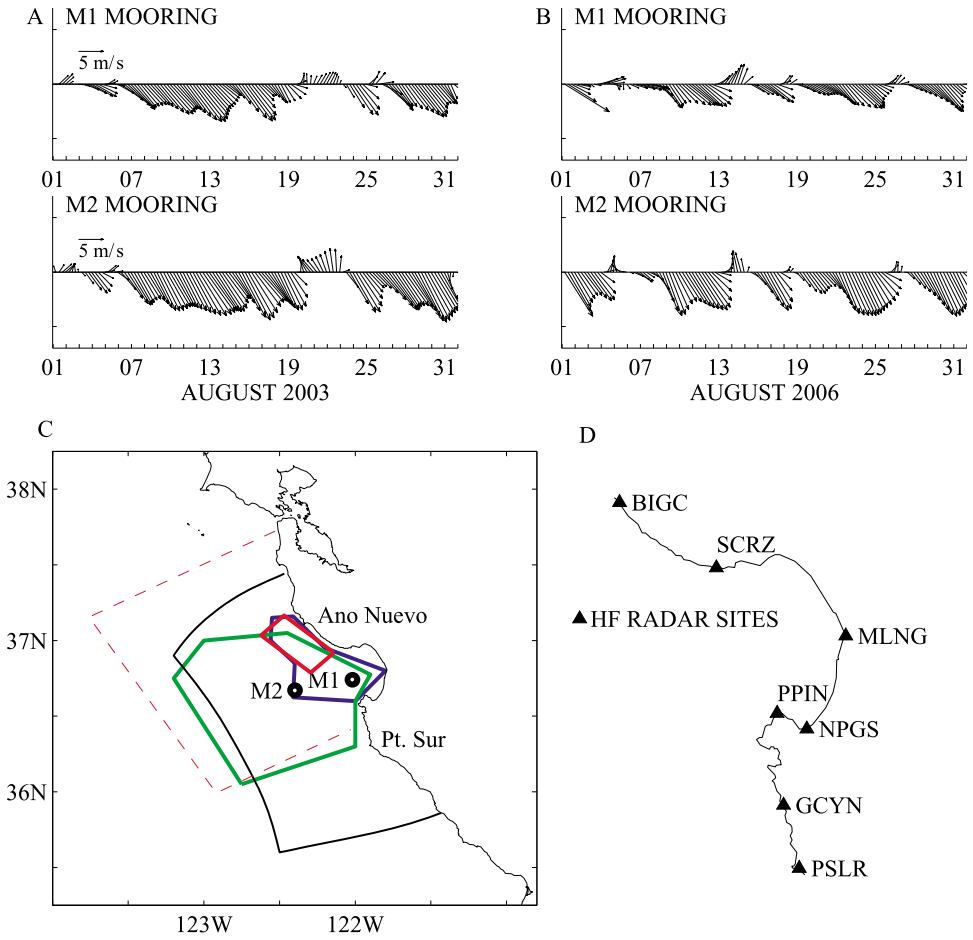

Figure 1. Observed wind velocities at M1 and M2 during (a) August 2003 and (b) August 2006. (c) M1 and M2 moorings locations, the NCOM ICON model domain (bounded by solid black line), areas sampled by Slocum (bounded by blue line) and Spray (bounded by green line) gliders in August 2003, the area sampled by gliders in August 2006 (bounded by solid red line), and the area of cruise surveys (bounded by dashed red line) are shown. (d) Locations of HF radar sites are shown.

al., 2005]. For this reason, the field program included an extensive sampling of the bay and surrounding areas with a fleet of underwater gliders, propeller-driven AUVs, a low-flying aircraft, HF Radars in addition to moorings, ships, and other more traditional observational techniques [*Ramp et al.*, 2009]. In contrast, the objectives of the 2006 experiment, called Adaptive Sampling and Prediction (ASAP), were more focused on the study of the properties of the upwelling center at Año Nuevo to the north of the Monterey Bay. For this reason, the extensive sampling was conducted inside of an approximately 1000 km^2 box in order to create a synoptic view of the oceanographic fields and fluxes in the upwelling center to the north of the Monterey Bay [*Bellingham and Rajan*, 2007].

[4] Objective of the present paper is to compare and discuss circulation patterns during upwelling/relaxation events of two field programs: the AOSN II (August 2003) and the ASAP (August 2006). Description and comparisons of upwelling/relaxation events provide the foundation for the presentation of the second paper's objective: to demonstrate the differences in impacts of glider data assimilation on the model's ability to simulate 2003 and 2006 events. As shown by *Shulman et al.* [2009], the Monterey Bay model was able to reproduce observed surface and subsurface features with assimilation of glider data from the extensive sampling of the bay and surrounding areas during the 2003 field program. In the present study, we investigate the impact of the upwelling center sampling during the ASAP (2006) experiment on the model simulations of observed properties to the south of the upwelling center.

[5] The structure of the paper is as follows: Section 2 describes observations and models. The comparison of circulation patterns of upwelling/relaxation events of 2003 and 2006 are presented in section 3. Section 4 is devoted to the Monterey Bay model results. Discussions and conclusions are presented in sections 5 and 6.

2. Methods

2.1. Observations

[6] Observations of winds, water velocity, temperature and salinity from the Monterey Bay Aquarium Research Institute (MBARI) surface moorings M1 (122.02°W, 36.74°N) and M2 (122.40°W, 36.67°N) are used in this

study (Figure 1). Each mooring has downward looking RD Instruments Inc. 75 KHz Acoustic Doppler Current Profiler (ADCP). In 2003 and 2006 deployments, ADCPs were set up to sample currents every 15 min in 60 8 m bins up to 500 m depth (the first bin at 16 m depth). Surface wind speed and direction were measured by a RM Young model 05103 wind monitor. Temperature and salinity were measured by Sea-Bird MicroCAT CTDs sensors at 12 depths between 1 and 350 m.

[7] Surface current observations used in this study were derived from a network of SeaSonde-type HF radar instruments deployed in the region of the Monterey Bay. Those instruments exploit information in the radio wave backscatter from the ocean surface to infer movement of the near surface water. Each individual SeaSonde instrument provides a distribution of "radial" velocity observations each hour on a polar coordinate grid centered on the radar site. Vector currents were estimated on a Cartesian grid with a horizontal resolution of 3 km by computing the best fit vector velocity components using all radial velocity observations within a radius of 3 km for each grid point each hour [*Paduan and Shulman*, 2004]. During the AOSN II experiment (2003), surface currents were estimated based on input from four HF radar sites (Figure 1): Santa Cruz (SCRZ), Moss Landing (MLNG), The Naval Postgraduate School (NPGS) and the Point Pinos (PPIN). During the ASAP (2006) experiment three more HF radar sites: Big Creek (BIGC), Granite Canyon (GCYN) and the Point Sur (PSUR) provided estimates of currents offshore. *Paduan et al.* [2006] investigated the performance of the Monterey Bay HF radar network by comparing the radar-derived currents with in situ velocity observations and by comparing radar-to-radar velocity estimates on the overwater baselines between radar sites. They reported error estimates for the HF radar-derived radials in the range of 7–9 cm/s.

[8] Daily mean sea level data for tide gauges stations at San Diego and Monterey Bay for a period of 1999–2006 were obtained from the NOAA tide gauges data set (http://tidesandcurrents.noaa.gov). Sea surface height (SSH) values from each tide gauge were adjusted by using atmospheric pressure sea level time series from the Coupled Ocean and Atmospheric Mesoscale Prediction System (COAMPS) [*Doyle et al.*, 2009; *Kindle et al.*, 2002] which is described in section 2.2.

[9] Five Spray gliders [*Sherman et al.*, 2001] and ten Slocum gliders [*Webb et al.*, 2001] were deployed in the AOSN II (2003) experiment in the Monterey Bay area [*Ramp et al.*, 2009]. Spray gliders collected temperature and salinity profiles up to 400 m depth (with occasional profiles to 700 m for instrument comparison with other measurements) from Point Año Nuevo in the north to Point Sur in the south, while the Slocum gliders profiled to 200 m closer to shore (Figure 1). During the ASAP (2006) experiment 4 Spray and 6 Slocum gliders were deployed in the area around Point Año Nuevo (Figure 1). Gliders collected temperature and salinity profiles in approximately 1000 km^2 domain (Figure 1).

[10] The R/V *Point Sur* occupied 69 hydrographic stations during the ASAP experiment (1–7 August 2006, Figure 1). Temperature and salinity depth profiles with 1 m vertical resolution were derived from Sea-Bird SBE 9+ CTD measurements using standard Sea-Bird processing software.

2.2. Models

[11] The Naval Research Laboratory has been developing a hierarchy of different resolution NCOM-based models on the West Coast of the United States [*Shulman et al.*, 2007]. The NCOM is a primitive equation, 3-D, hydrostatic model. It uses the Mellor-Yamada level 2.5 turbulence closure scheme, and the Smagorinsky formulation for horizontal mixing [*Martin*, 2000].

[12] The NCOM global model [*Rhodes et al.*, 2002; *Barron et al.*, 2004] has 1/8° horizontal resolution and the model assimilates satellite-derived SSH and sea surface temperature (SST) data via synthetic temperature and salinity profiles derived from the Modular Ocean Data Assimilation System (MODAS [*Fox et al.*, 2002]), and uses atmospheric forcing from the Navy Global Atmospheric Prediction System (NOGAPS [*Rosmond et al.*, 2002]). The Global NCOM provides boundary conditions for the NCOM-based regional model of the California Current (NCOM CCS [*Shulman et al.*, 2007]). The NCOM CCS has a horizontal resolution of about 9 km and as in the global model, the NCOM CCS assimilates satellite-derived SSH and SST data via synthetic temperature and salinity profiles derived from the MODAS. The NCOM CCS model is forced with atmospheric products derived from the Coupled Ocean and Atmospheric Mesoscale Prediction System (COAMPS) [*Doyle et al.*, 2009].

[13] The COAMPS atmospheric model is a finite difference approximation to the fully compressible, nonhydrostatic equations [*Doyle et al.*, 2009]. The domain configuration contains four horizontally nested grid meshes of 81 km, 27 km, 9 km, and 3 km, respectively. The 3 km resolution grid mesh is centered over Central California and the Monterey Bay. COAMPS assimilates atmospheric observations from radiosondes, aircraft, satellite and ships [*Doyle et al.*, 2009]. The data assimilation is accomplished through an incremental update procedure that enables mesoscale phenomena to be retained in the analysis increment fields. Results of COAMPS evaluation and verification are presented by *Kindle et al.* [2002], *Doyle et al.* [2009], and *Shulman et al.* [2007, 2009].

[14] The regional NCOM CCS provides boundary values to the high-resolution NCOM model of the Monterey Bay Area. The model is called NCOM ICON [*Shulman et al.*, 2007], and it is set up on a curvilinear orthogonal grid with resolution ranging from 1 to 4 km. There are 30 sigma coordinate vertical levels. The NCOM ICON model domain is shown on Figure 1. The NCOM ICON model is forced with surface fluxes from the COAMPS atmospheric model at 3 km horizontal resolution. The Navy Coupled Ocean Data Assimilation (NCODA) system [*Cummings*, 2006] is used for the assimilation of the glider temperature and salinity data [*Shulman et al.*, 2009]. The NCODA is a fully 3D multivariate optimum interpolation system. Assimilation of temperature and salinity data is performed every 12 h (assimilation cycle). Differences between the NCODA analysis and the model forecast are uniformly added to the model temperature and salinity fields over the assimilation

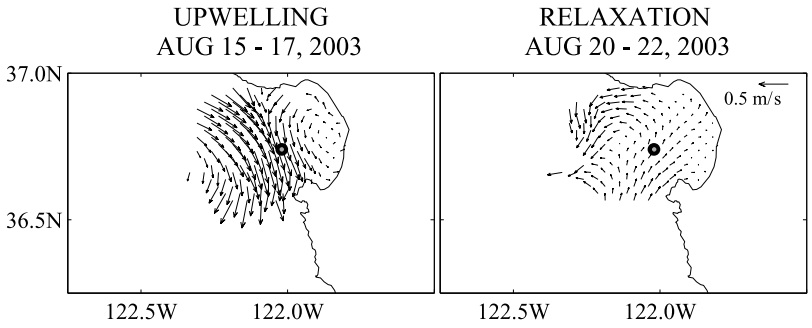

Figure 2. HF radar surface currents averaged over (left) 3 days of upwelling and (right) 3 days of relaxation in August 2003.

cycle. The evaluation of the NCOM Monterey Bay model predictions are presented by *Shulman et al.* [2007, 2009].

3. Upwelling and Relaxation Events During August 2003 and 2006

[15] During northwesterly, upwelling favorable winds, the mesoscale and large-scale features in and around the Monterey Bay are mostly determined by the interaction between upwelling filaments formed at headlands to the north (Pt. Año Nuevo, Figure 1) and to the south of the bay (Pt. Sur) and by the California Current system offshore of the bay [*Rosenfeld et al.*, 1994]. The development and intensification of a southward flowing jet and pair of cyclonic (inside of the bay) and anticyclonic (outside of the bay) circulations were often observed during upwelling events. During relaxation events, the upwelling favorable winds weaken and sometimes reverse. The anticyclonic California Current meander moves onshore, and the currents on the continental shelf become poleward (see, for example, *Rosenfeld et al.* [1994] and *Ramp et al.* [2005] for more details).

[16] Figure 1 shows the observed wind velocities at the MBARI moorings M1 and M2. The wind time series were 33 h low-pass filtered and plotted each 6 h. According to the Figure 1, there was an extended upwelling event during 7–19 August 2003 followed by a brief relaxation event during 20–22 August. The spatial distribution of the HF radar derived surface currents, averaged over 3 days of upwelling (15–17 August) and 3 days of relaxation (20–22 August), are shown on Figure 2. Figure 3 shows the subsurface profiles of northward and eastward velocity components at mooring M1. Profiles are averaged over the same days of upwelling and relaxation as HF radar derived surface currents on Figure 2. During the upwelling event, Figure 2 indicates the development of strong southward flowing jet at the surface, which extends up to 150 m depth (Figure 3, negative values of V component indicate southward flow). The development of the southward flowing jet along the entrance to the bay is a typical feature during observed upwelling events [*Rosenfeld et al.*, 1994; *Ramp et al.*, 2005, 2009]. The southward jet brings cold, nutrient-rich upwelled water from the upwelling center at Año Nuevo to the mouth of the bay. The water bifurcates, such that some water flows offshore and some into the bay [*Rosenfeld et al.*, 1994]. During the relaxation period, when upwelling favorable winds weaken, the structure of the currents is more complicated yet there is a clear indication of the development of an alongshore northward flow at the surface (Figure 2) and the subsurface (Figure 3) near the entrance to the bay. This northward flow during the relaxation event is much weaker than the southward flowing jet associated with the upwelling (Figures 2 and 3).

[17] During August 2006, there was a short relaxation event (4-6 August) followed by an upwelling event during 8–12 August, which was followed with another relaxation event during 13–15 August (Figure 1b). Figure 4 presents HF radar derived surface currents averaged over 3 days of upwelling (10–12 August) and over above mentioned

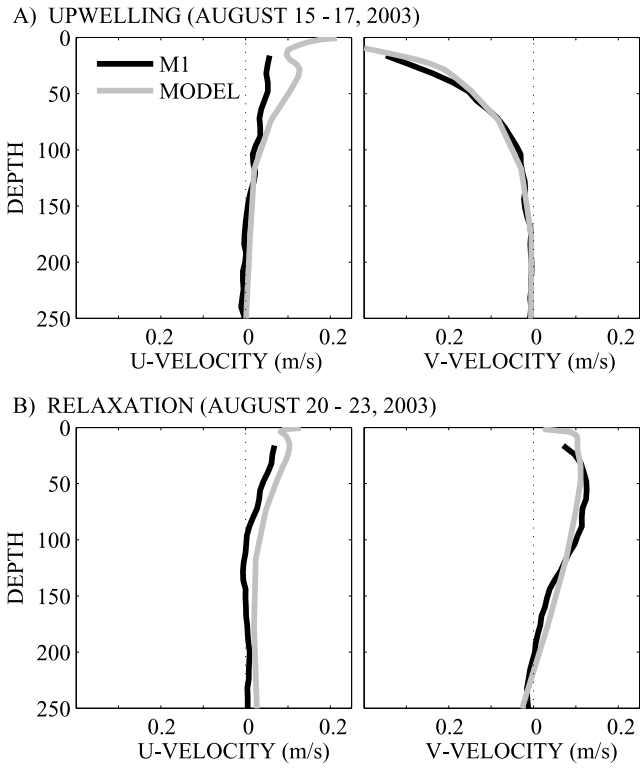

Figure 3. ADCP observed (black line) and the NCOM ICON model predicted (gray line) subsurface profiles of the velocity components at the M1 mooring. Profiles are averaged over upwelling and relaxation events. U is the eastward and V is the northward component of velocity.

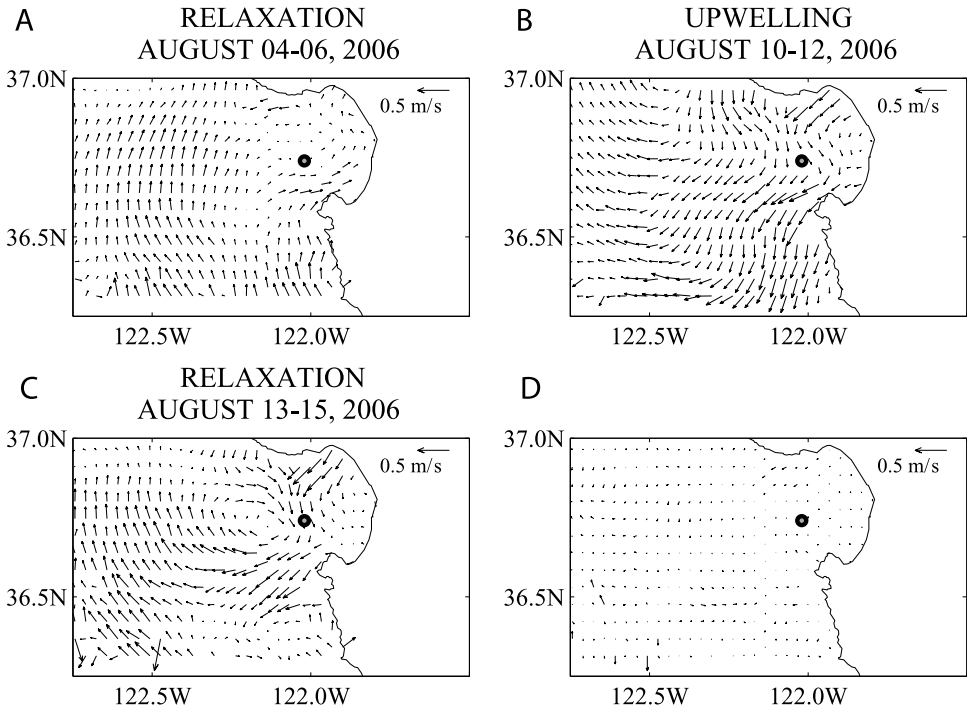

Figure 4. HF radar surface currents averaged over (b) upwelling and (a and c) two relaxation events in August 2006. (d) Differences in circulation patterns between averaging over 3 (13–15 August) and 2 (14–15 August) days of the relaxation event are shown.

relaxation events. Subsurface currents at mooring M1 are shown on Figure 5. The southward jet is much weaker, less organized and shallower during the upwelling event of 2006 than in 2003.

[18] During the first relaxation event, surface HF radar currents (Figure 4) and subsurface currents (Figure 5) show similarities with the relaxation event of 2003 (Figures 2 and 3). There is a development of a northward flow up to the 200 m depth. However, the second relaxation event of 2006 (13–15 August) is significantly different from the first event and from the relaxation event of 2003. HF radar surface currents show a southward flow along the entrance to the bay, separating the cyclonic eddy inside the bay and an anticyclonic one outside of the bay (which is typical circulation pattern for the upwelling event). The southward jet, during the second relaxation event, penetrates to around 50 m depth (Figure 5). There is no development of a northward flow during this relaxation event. To avoid the possibility that the anomalous currents structure of the relaxation event is the result of too early an averaging, the HF radar surface currents were also averaged over 2 days of relaxation (14–15 August). Figure 4 shows that differences in circulation patterns between averaging over 3 (13–15 August) and 2 (14–15 August) days are insignificant.

[19] The contrast and differences between upwelling/relaxation events of 2003 and 2006 are illustrated on Figure 6. The 33 h low-pass filtered north-south wind component at M1, as well as the 3 day moving average velocity at M1 for August 2003 and 2006 is shown. During August 2003, there is development of a southward flow, penetrating into the subsurface during upwelling favorable winds, and northward flow (also penetrating into subsur-

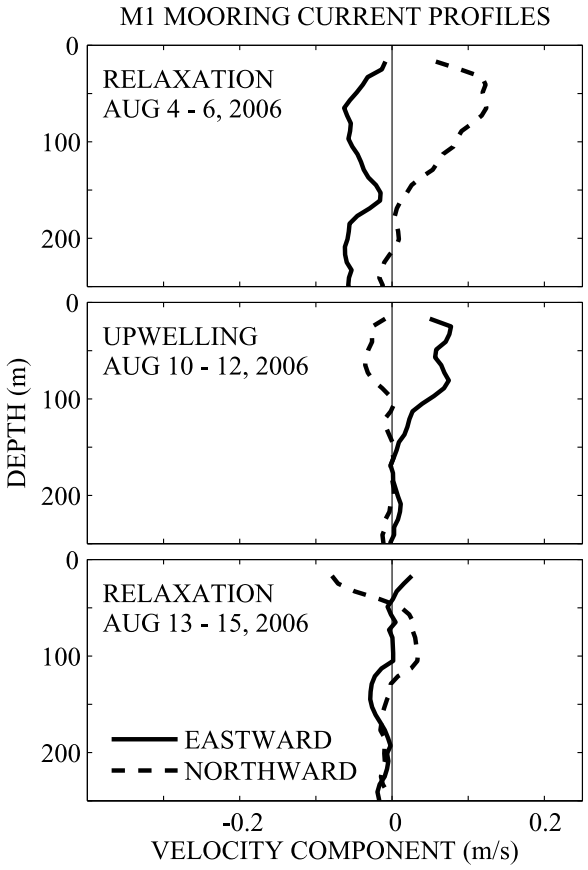

Figure 5. ADCP observed velocity profiles at M1 averaged over upwelling and relaxation events of August 2006.

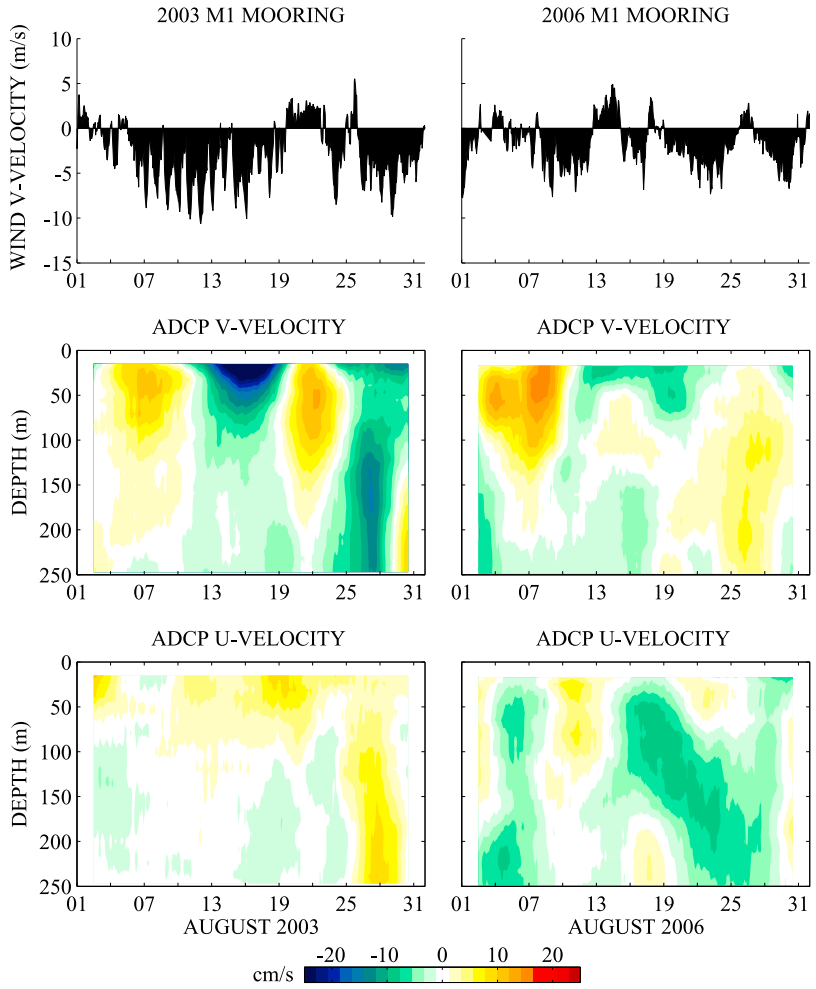

Figure 6. (top) North-south wind velocity component, as well as (middle) northward and (bottom) eastward components of ADCP velocity at mooring M1 for (left) August 2003 and (right) August 2006. Wind velocities are 33 h low-pass filtered, and ADCP velocities are 3 day moving averaged.

face) during relaxation of winds. However, during August 2006, while there is a northward flow during the first relaxation event (4–6 August), there is weak and shallow southward flow during the upwelling event of 2006.

[20] Table 1 presents means of observed winds at mooring locations averaged over considered upwelling and relaxation events of 2003 and 2006. The upwelling favorable winds were weaker during the 2006 event than during the 2003 event. The weaker upwelling favorable winds and shorter upwelling during 2006 compared to 2003 (Table 1 and Figure 6) is one of the reasons for observed above differences in circulation patterns. Another reason is the presence of a strong remote forcing during August 2006. Figure 7a shows the latitude-time diagram of SSH anomalies along the coast for July–September 2006, derived from the global NCOM model [*Rhodes et al.*, 2002; *Barron et al.*, 2004] described in section 2.2. The anomalies are estimated with respect to the model mean over 1999–2007 and include seasonal cycle. The latitude-time diagram shows the propagation of positive SSH anomalies along the coast during July–August 2006 (the *y* axis label has latitude 25N twice in order to show the wave traveling through the Gulf of California). Many previous studies documented poleward propagation of the SSH anomalies along the West Coast [e.g., *Chelton and Davis*, 1982; *Enfield and Allen*, 1980; *Spillane et al.*, 1987]. The estimated phase speed of propagation by the slope of the maxima in latitude versus time plot (Figure 7a) is about 2–3.5 m/s, which is in agreement with previous estimates of phase speed for the first baroclinic coastally trapped Kelvin wave [*Enfield and Allen*, 1980; *Spillane et al.*, 1987]. The model results indicate the

Table 1. Wind Magnitude Means at M1 and M2 During Upwelling and Relaxation Periods of August 2003 and 2006[a]

	Mooring M1	Mooring M2
15–17 Aug 2003 (up)	6.24	8.94
20–22 Aug 2003 (re)	2.39	3.60
4–6 Aug 2006 (re)	3.02	2.79
10–12 Aug 2006 (up)	5.86	7.40
13–15 Aug 2006 (re)	3.53	2.96

[a]Wind magnitude is given in m/s. Here up means upwelling and re means relaxation.

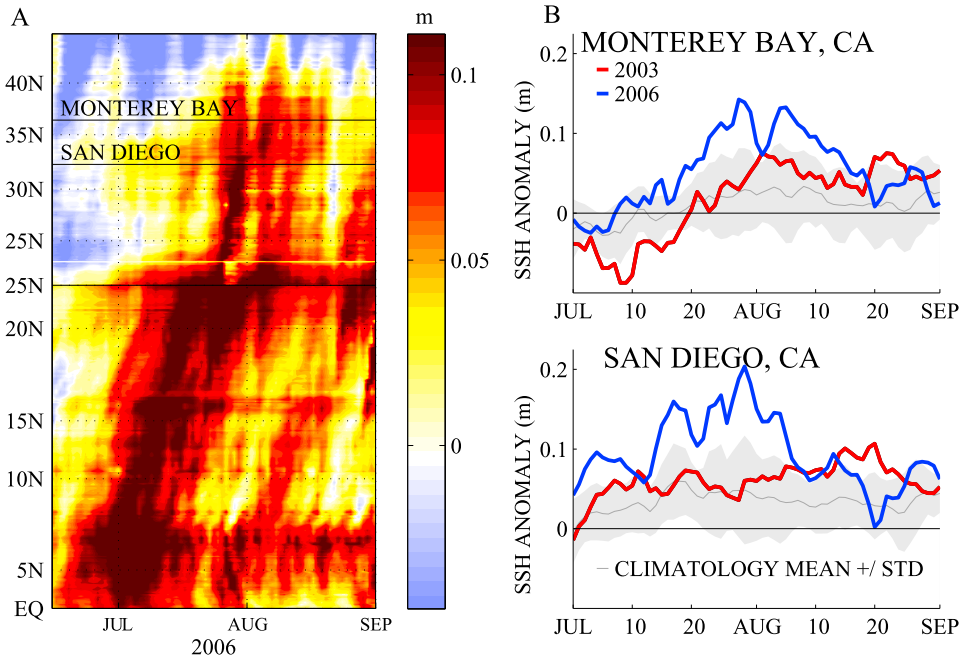

Figure 7. (a) A latitude-time diagram of surface height anomalies along the coast derived from the global NCOM model (the *y* axis label has latitude 25°N twice in order to show the wave traveling through the Gulf of California). (b) Tide gauge observations at (top) Monterey Bay and (bottom) San Diego for July–August 2003 (red line) and 2006 (blue line) over climatological mean (black line) and standard deviation (shaded area).

equatorial origin of positive SSH anomalies. Figure 7b shows the observed sea surface height anomalies at tide gauges at San Diego and Monterey stations. Figure 7b also shows the mean of observed SSH over 1999–2006 and the standard deviation from the mean. The observed SSH during July–August 2006 are much higher than the mean value and are outside of standard deviation from the mean. The maximum SSH is reached around the beginning of August.

[21] Two reasons for the observed 2003 and 2006 differences are outlined here: weaker winds in August 2006 than in the August 2003 and strong positive SSH anomalies propagating poleward along the coast during 2006. Other physical processes controlling local dynamics in the Monterey Bay which could contribute to the observed differences are not discussed here.

4. Impact of Glider Data Assimilation on the Monterey Bay Model Predictions

[22] As shown by *Shulman et al.* [2009], the Monterey Bay model was able to reproduce observed surface and subsurface features with assimilation of glider observations during the AOSN II (2003) field program. For the ASAP 2006 experiment, three model runs are considered here: the run 1 without assimilation, the run 2 with assimilation of only glider temperature and salinity data and the run 3 with assimilation of temperature and salinity from gliders and cruises profiles. Figure 8 shows comparisons of subsurface temperature and salinity from the model and observations at mooring M1. Table 2 presents estimates of anomaly correlation (AC) and root mean square error (RMSE) between observed and model subsurface temperature and salinity profiles (Figure 8). Anomaly correlation is estimated from

$$\mathrm{AC} = \frac{\sum_G (M-\overline{M})(O-\overline{O})}{\sqrt{\sum_G (M-\overline{M})^2}\sqrt{\sum_G (O-\overline{O})^2}},$$

where M and O are corresponding model and observed temperature or salinity profiles, $\overline{M}$ and $\overline{O}$ are means over time of observed and model subsurface temperature or salinity profiles, and G denotes the number of grid points. The summation is performed over depth and time. The root mean square (RMS) is estimated from

$$\mathrm{RMS} = \sqrt{\frac{1}{G}\sum_G (M-O)^2}.$$

The NCOM ICON model predictions of temperature and salinity with assimilation of glider data are very close to predictions for the run without assimilation (Figure 8). This is also reflected well in estimated values of AC and RMS (Table 2). Therefore, the assimilation of the glider temperature and salinity data from the upwelling center at Pt. Año Nuevo (Figure 1c) has minimal impact on the model predictions around the mooring location. Only with assimilation of temperature and salinity profiles from cruise surveys (covering the M1 area) the model was able to reproduce the observed subsurface structure of the temperature and salinity.

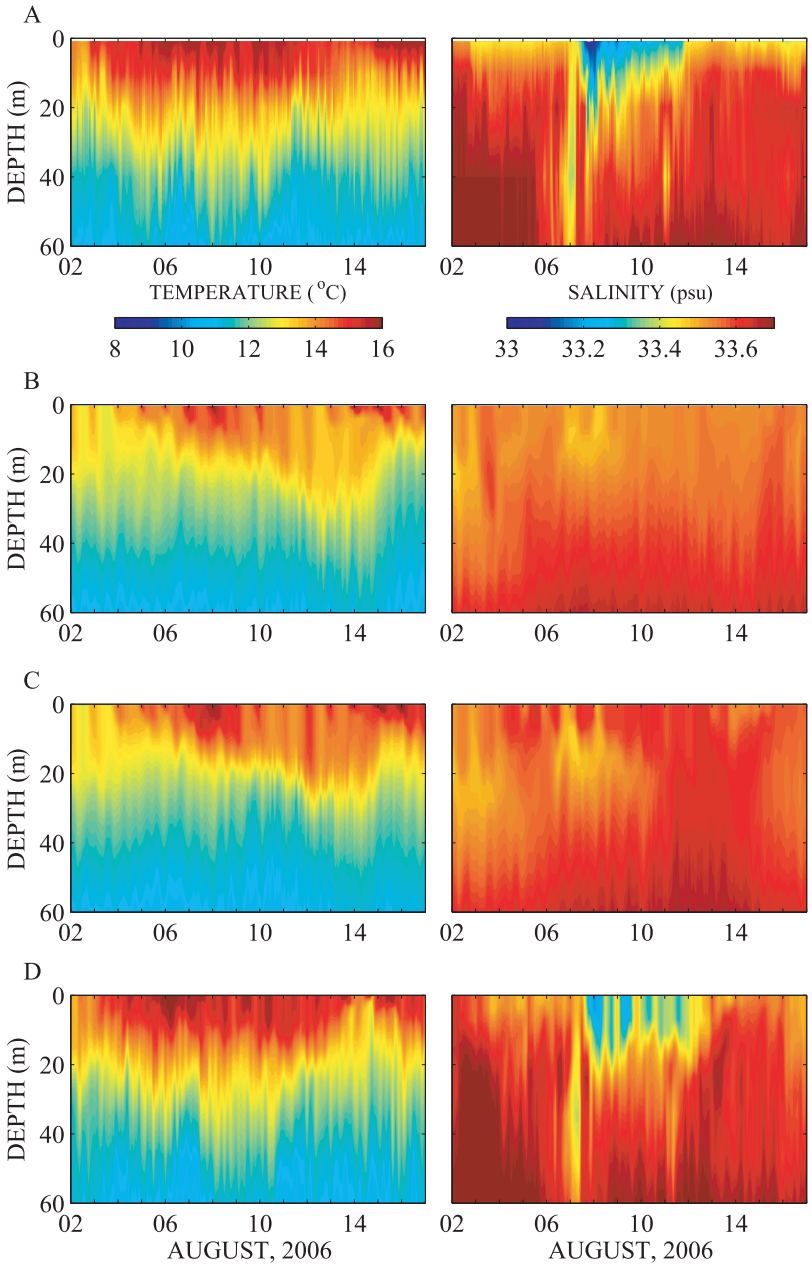

Figure 8. Comparison of observed and model-predicted subsurface temperature and salinity at mooring M1 during August 2006: (a) observed, (b) no assimilation, (c) with assimilation of glider data, and (d) with assimilation of glider data and cruise surveys.

[23] The above three model runs have poor visual agreement of surface currents (not shown here) with the spatial distributions of HF radar derived surface currents (Figure 4). The magnitude ρ and the angular displacement θ of the complex correlation coefficient between the mooring M1 ADCP and the model currents for a particular depth are estimated using the approach outlined by *Kundu* [1976]. The model currents averaged over 3 × 3 horizontal grids around the mooring location. The magnitude is estimated as

$$\rho = \sqrt{\mathrm{Re}^2 + \mathrm{Im}^2}, \qquad (1)$$

Table 2. AC and RMS for Temperature and Salinity at M1 for 2–17August 2006

	Temperature		Salinity	
	AC	RMS	AC	RMS
No assimilation	0.272	0.912	0.068	0.169
With glider assimilation	0.226	0.786	−0.033	0.183
With glider and cruise data assimilation	0.463	0.524	0.428	0.143

Table 3. Magnitude of Complex Correlation and the Angular Displacement Between the Mooring M1 ADCP and the Model Currents

Depth	Complex Correlation (ρ)	Angular Displacement (θ)
16 m	0.25	107°
32 m	0.2	142°
48 m	0.08	113°
64 m	0.09	67°
120 m	0.15	64°
240 m	0.25	98°

where

$$\mathrm{Re} = \frac{\sum_t \left(u_t^o u_t^m + v_t^o v_t^m\right)}{\sqrt{\sum_t \left(\left(u_t^o\right)^2 + \left(v_t^o\right)^2\right) \sum_t \left(\left(u_t^m\right)^2 + \left(v_t^m\right)^2\right)}},$$

$$\mathrm{Im} = \frac{\sum_t \left(u_t^o v_t^m + v_t^o u_t^m\right)}{\sqrt{\sum_t \left(\left(u_t^o\right)^2 + \left(v_t^o\right)^2\right) \sum_t \left(\left(u_t^m\right)^2 + \left(v_t^m\right)^2\right)}}.$$

[24] The corresponding angular displacement θ, which is also called the phase angle, is computed according to

$$\theta = \tan^{-1} \frac{\sum_t \left(u_t^o v_t^m - v_t^o u_t^m\right)}{\sum_t \left(u_t^o u_t^m + v_t^o v_t^m\right)}, \qquad (2)$$

where u_t^m, v_t^m are the demeaned east-west and north-south model velocity components, respectively, and u_t^o, v_t^o are the demeaned east-west and north-south observed velocity components, respectively. The angular displacement θ gives the average counterclockwise angle difference between model and observed velocity vectors. The value of θ is only meaningful if ρ is significant. Correlations are estimated over a 15 day period (1–15 August 2006) using hourly model and observed data passing through a 33 h low-pass filter. Therefore, the actual number of degrees of freedom is less or equal to $15 \times 24/33 \approx 11$. With 11 degrees of freedom, a correlation 0.6 is significant at 95% confidence level [see, e.g., *Wilks*, 1995]. Therefore, correlations less than 0.6 should be considered as insignificant. Table 3 shows correlations and angular displacements with observed currents for the described above run 3. The values of complex correlations are below the significance level for all considered depths.

5. Discussions

[25] Two reasons for the observed differences in upwelling and relaxation events of 2003 and 2006 are discussed in section 3: weaker winds in August 2006 than in the August 2003 and strong positive SSH anomalies propagating poleward along the coast during 2006. At the same time, there are other physical processes controlling local dynamics in the Monterey Bay which could contribute to the differences in upwelling/relaxation events described in section 3. These include meandering eddies, California Current system, internal tides, land/sea breeze processes etc. [see, e.g., *Ramp et al.*, 2005].

[26] However, the limited in space (Figure 1c) and time sampling during the ASAP 2006 experiment alleviate possibility of the comprehensive analysis of these processes.

[27] Models can provide additional insights in situation when observations are limited. However, as was demonstrated in section 4, the level of the Monterey Bay model fidelity in simulating events of 2003 and 2006 is quite different between years. During 2003, the model with assimilation of observations was able to reproduce observed surface and subsurface features. However, during 2006 the model fidelity is very low, which limits the possibility of its use in describing 2006 events. One of the reasons for the model poor fidelity during 2006 is the sampling strategy and coverage with gliders, when during the entire field program all tracks were concentrated in the small box covering the upwelling center to the north (Figure 1c). As demonstrated in section 4, sampling of the upwelling center with gliders has minimal impact on the model's ability to simulate observed subsurface structure of temperature and salinity in 2006.

[28] This can be illustrated and supported by the model-derived passive tracer adjoint distributions maps described in Appendix A. As shown in Appendix A, the adjoint tracer

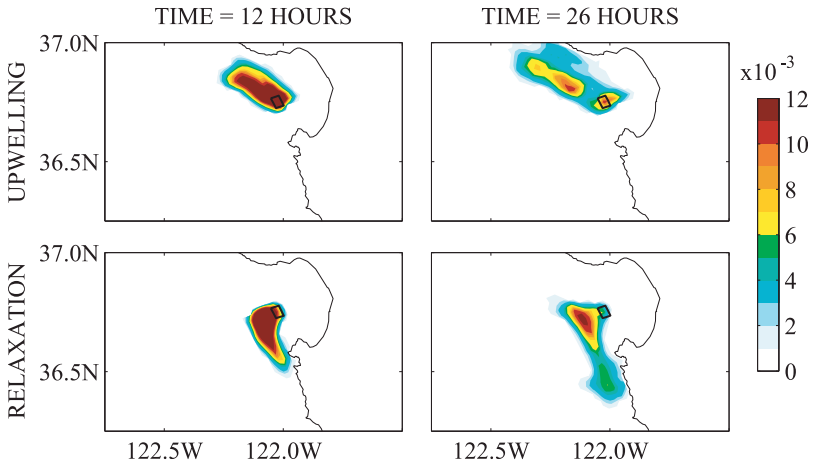

Figure 9. Adjoint sensitivities maps for upwelling and relaxation events in 2003.

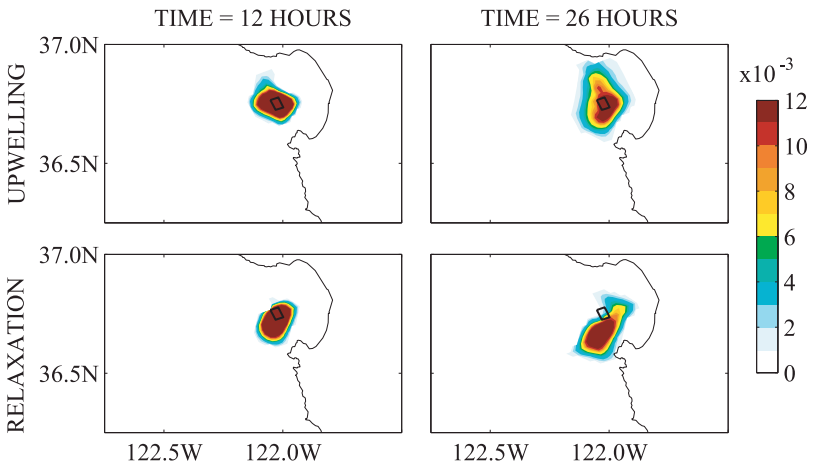

Figure 10. Adjoint sensitivities maps for upwelling and relaxation events in 2006.

distributions show where the model water masses, tagged by the passive tracer, are coming from to the area of interest (like, for example, the area around the mooring M1 location). Therefore, they show domains which are important for sampling as indicated by the model. Figures 9 and 10 show adjoint tracer distribution maps for upwelling and relaxation events of 2003 and 2006. The passive tracer adjoint patterns show distinct differences in the origin and pathways of the model water masses during the upwelling/relaxation events of 2003 and 2006. In 2003, for the upwelling event (Figure 9 (top)) the adjoint tracer is spread to the north of the mooring location, indicating the importance of the upwelling center sampling. In contrast to 2003, the model tracer adjoint maps for 2006 events (Figure 10) are more centered around the mooring area, and they are not extended to the area of the northern upwelling center. During the relaxation events of 2003 and 2006 (Figures 9 and 10 (bottom)), the highest values of the adjoint are spread to the south (more in 2003 than in 2006), southeast of the target area. In contrast to the AOSN II (2003) experiment, the model adjoint tracer distribution areas were not sampled by the gliders during the ASAP 2006 experiment (Figure 1c), which explains the minimal impact of the glider data assimilation on the Monterey Bay model results during August 2006.

6. Conclusions

[29] Observations show significant differences in circulation patterns of upwelling and relaxation events that occurred in the Monterey Bay during Augusts 2003 and 2006. During 2003, observed circulation exhibited more typical patterns associated with upwelling/relaxation: the development of the southward flowing jet and a pair of cyclonic (inside of the bay) and anticyclonic (outside of the bay) circulations during upwelling, and development of the northward flow along the coast during relaxation of winds. This northward flow during the relaxation event is weaker than the southward flowing jet associated with the upwelling (Figures 2 and 3).

[30] During the upwelling event of 2006, the southward flow was weaker and shallower than in 2003, and there was a strong northward flow during the first relaxation event. The second relaxation event of 2006 was significantly different from the first relaxation event of 2006 and the relaxation event of 2003: a southward flow is present along the entrance to the bay, and this southward flow penetrates into the subsurface up to around 50 m at mooring M1. There is no development of northward flow during the second relaxation event.

[31] Two reasons for the observed differences in upwelling and relaxation events of 2003 and 2006 are identified in the paper: weaker winds in August 2006 than in the August 2003 and strong positive SSH anomalies propagating poleward along the coast during 2006. The estimated phase speed of propagation of these anomalies is in agreement with phase speed for the first baroclinic coastally trapped Kelvin wave. The NCOM global model results indicate the equatorial origin of these positive SSH anomalies.

[32] The 2003 field program included an extensive sampling of the bay and surrounding areas with a fleet of underwater gliders, while during the 2006 program, extensive sampling was conducted in the area of the upwelling center to the north of the Monterey Bay. The Monterey Bay model's ability to reproduce observed features during upwelling/relaxation events was quite different between the 2 years. During the 2003 field program, the model was able to reproduce observed surface and subsurface features with assimilation of glider observations. However, during 2006 field program, the assimilation of glider data from the upwelling center to the north of the bay had minimal impact on model simulations of observed features to the south of the upwelling center.

Appendix A

A1. Passive Tracer and Its Adjoint

[33] Consider the passive tracer equation for concentration $C(x,y,z,t)$

$$\frac{\partial C}{\partial t} = -u\frac{\partial C}{\partial x} - v\frac{\partial C}{\partial y} - w\frac{\partial C}{\partial z} + \frac{\partial}{\partial \mathrm{x}}\left(\mathrm{A}\frac{\partial \mathrm{C}}{\partial \mathrm{x}}\right) + \frac{\partial}{\partial \mathrm{y}}\left(\mathrm{A}\frac{\partial \mathrm{C}}{\partial \mathrm{y}}\right) + \frac{\partial}{\partial \mathrm{z}}\left(\mathrm{K}\frac{\partial \mathrm{C}}{\partial \mathrm{z}}\right), \tag{A1}$$

with initial conditions at time t = t_0

$$C = C_0,$$

where diffusivities (A and K) and velocities (u,v,w) are from the NCOM ICON model described in section 2.2. Lets consider the following objective function J at time t > t_0

$$J = \frac{\int\limits_V C(\tau,t)d\tau}{\int\limits_V d\tau}, \quad \text{(A2)}$$

where V is a particular subdomain (target area) of the modeling domain, τ is the location in the model domain with coordinates (x,y,z), and $d\tau$ is a volume element. Therefore, function J is the normalized content of tracer C in the domain V at time t.

[34] By using the adjoint for the tracer equation (1), the gradient of the function J (equation (A2)) at time t with respect to the initial concentration C_0 at time t_0, can be estimated

$$s = \frac{\partial J}{\partial C_0}, \quad \text{(A3)}$$

where s is the sensitivity, $\partial J/\partial C_0$ is the gradient of J (at time t) with respect to initial conditions C_0. Sensitivity, s, is a function of x, y, z and times, t_0 and t, and can be estimated by seeding the adjoint variable with a unit value at each grid point in the volume V at time t, and integrating the adjoint of the tracer model backward in time to time t_0 [*Baker and Daley*, 2000; *Rabier et al.*, 1996; *Fukumori et al.*, 2004; *Shulman et al.*, 2005]. The function $s(x, y, z, t)$ is called the adjoint tracer sensitivity, as well as the adjoint tracer distribution (because the function s, is the result of the adjoint tracer model integration).

A2. Interpretation of the Adjoint Tracer Distribution

[35] Lets introduce some finite perturbation ΔC_0 at location $X_0 = \{ x_0, y_0, z_0\}$ to the initial concentration C_0 at time t_0, according to (A3) we would have

$$\Delta J = s(x_0, y_0, z_0, t_0, t) \cdot \Delta C_0. \quad \text{(A4)}$$

According to (A2) and (A4), the adjoint tracer distribution s (x_0, y_0, z_0, t_0, t) represents a fraction of tracer ΔC_0, which makes its way to the volume V from time t_0 to time t. Due to the linearity of the passive tracer and its adjoint problems, the adjoint tracer distribution $s(x, y, z, t_0, t)$ will represent the fraction of the tracer-tagged water that makes its way from location (x, y, z) at time t_0 to the volume V at time t [see also *Fukumori et al.*, 2004]. Therefore, the adjoint tracer distribution provides information on the model tracer history and identifies origin and pathways of the model tracer-tagged water masses in the past, which circulated into the target area, and therefore contain useful information about model circulation patterns and the propagation of information within the system. In this case, the adjoint tracer distribution (sensitivity) maps show areas which are important for sampling in order to improve the model tracer predictions at the target area. Note, that while adjoint tracer distribution shows areas where additional sampling is most influential, they do not necessarily show where additional observations will improve the forecast [*Baker and Daley*, 2000]. In order to improve the forecast, observations have to go through the data assimilation system, and the derivation of adjoint sensitivity maps does not consider such elements of the data assimilation system as, for example, errors in the background field and observations, and their corresponding error covariances.

A3. Adjoint Tracer Distributions for Upwelling and Relaxation Events of 2003 and 2006

[36] The adjoint tracer distributions ((A1) and (A2)) are estimated for upwelling and relaxation events of 2003 and 2006. For volume V in (A2), the model subdomain consisting of 3 by 3 horizontal grids around the mooring M1 and depth down to 300 m is considered. In this case the adjoint passive tracer distributions (A3) show areas from which model tracer-tagged water masses at time t_0 will be advected and mixed into the target area (around mooring M1) at time $t > t_0$. Figure 9 shows vertically integrated adjoint tracer maps for upwelling and relaxation events of 2003. For upwelling, the adjoint tracer distributions are estimated at time t equals 17 August 2003 0000 UT, and for relaxation at time t equals 22 August 2003 0000 UT. The adjoint tracer maps are shown for 12 and 26 h prior to the time t. Figure 10 shows the adjoint tracer maps for upwelling and relaxation events of 2006. For the upwelling event of 2006, adjoint sensitivities are estimated at time t equal 11 August 2006 0000 UT, and for relaxation at time t equals 6 August 2006 0000 UT. As for 2003, sensitivity maps are shown for 12 and 26 h prior to the time t. Note, that the derived above adjoint distributions for passive tracers will generally differ from the adjoint distributions for the dynamically active tracers as temperature and salinity. However, some similarities between passive tracer and dynamically active tracer adjoint distribution maps can be expected, especially if we consider relatively short time periods as 12 to 26 h, not several days.

[37] For example, with the development of a southward jet during upwelling and poleward flow during relaxation in 2003, the Figure 9 shows expansion to the north (during upwelling) or to the south (during relaxation) of the adjoint distribution maps for the passive tracer. Similar features can be expected for the adjoint distribution maps for the active model dynamical tracers as temperature and salinity.

[38] **Acknowledgments.** This research was funded through the Naval Research Laboratory (NRL) 6.1 project, "Bio-optical studies of predictability and assimilation in the coastal environment" under program element 61153N and grants N0001408WX21037 and N0001407WX20587 sponsored by the Office of Naval Research. We are grateful to the whole AOSN team and especially Jim Bellingham, Naomi Leonard, Francisco Chavez, Russ Davis, and Dave Fratantoni for discussions and their collaborations. We thank Jeff Paduan of NPS for collaborations on HF Radar surface currents, and Dmitri Nechaev of USM for helpful discussions about adjoint. Mooring data were provided by Francisco Chavez of MBARI. We thank Peter Sakalaukus of USM for programming and computer support, and we thank Mike Cook and Fred Bahr of NPS for providing assistance with the quality control and processing of the HF Radar and mooring data. We thank anonymous reviewers provided very insightful comments and recommendations to improve the paper. Computer time for the numerical simulations was provided through a grant from the Department of Defense High Performance Computing Initiative. This manuscript is NRL contribution 7330-08-8234.

References

Baker, N. L., and R. Daley (2000), Observation and background adjoint sensitivity in the adaptive observation-targeting problem, *Q. J. R. Meteorol. Soc.*, *126*, 1431–1454, doi:10.1256/smsqj.56510.

Barron, C. N., A. B. Kara, H. E. Hurlburt, C. Rowley, and L. F. Smedstad (2004), Sea surface height predictions from the Global Navy Coastal Ocean Model (NCOM) during 1998–2001, *J. Atmos. Oceanic Technol.*, *21*, 1876–1894, doi:10.1175/JTECH−1680.1.

Beardsley, R. C., and S. J. Lentz (1987), The Coastal Ocean Dynamics Experiment collection: An introduction, *J. Geophys. Res.*, *92*, 1455–1463, doi:10.1029/JC092iC02p01455.

Bellingham, J. G., and K. Rajan (2007), Robotics in remote and hostile environments, *Science*, *318*, 1098–1102, doi:10.1126/science.1146230.

Chelton, D. B., and R. E. Davis (1982), Monthly mean sea level variability along the west coast of North America, *J. Phys. Oceanogr.*, *12*, 757–784, doi:10.1175/1520-0485(1982)012<0757:MMSLVA>2.0.CO;2.

Cummings, J. A. (2006), Operational multivariate ocean data assimilation, *Q. J. R. Meteorol. Soc.*, *131*, 3583–3604, doi:10.1256/qj.05.105.

Doyle, J. D., Q. Jiang, Y. Chao, and J. Farrara (2009), High-resolution atmospheric modeling over the Monterey Bay in support of the AOSNII field campaign, *Deep Sea Res. Part II*, *56*, 87–99, doi:10.1016/j.dsr2.2008.08.009.

Enfield, D. B., and J. S. Allen (1980), On the structure and dynamics of monthly mean sea level anomalies along the Pacific coast of North and South America, *J. Phys. Oceanogr.*, *10*, 557–578, doi:10.1175/1520-0485(1980)010<0557:OTSADO>2.0.CO;2.

Fox, D. N., C. N. Barron, M. R. Carnes, M. Booda, G. Peggion, and J. Van Gurley (2002), The Modular Ocean Data Assimilation System, *Oceanography*, *15*(1), 22–28.

Fukumori, I., T. Lee, B. Cheng, and D. Menemenlis (2004), The origin, pathway, and destination of Nino-3 water estimated by a simulated passive tracer and its adjoint, *J. Phys. Oceanogr.*, *34*, 582–604, doi:10.1175/2515.1.

Kindle, J. C., R. Hodur, S. deRada, J. Paduan, L. K. Rosenfeld, and F. P. Chavez (2002), A COAMPS^{TM} reanalysis for the eastern Pacific: Properties of the diurnal sea breeze along the central California coast, *Geophys. Res. Lett.*, *29*(24), 2203, doi:10.1029/2002GL015566.

Kundu, P. K. (1976), Ekman Veering observed near the ocean bottom, *J. Phys. Oceanogr.*, *6*, 238–242.

Martin, P. J. (2000), Description of the Navy Coastal Ocean Model version 1.0, *Rep. NRL/FR/732-00-9962*, Nav. Res. Lab., Stennis Space Center, Miss.

Moline, M. A., S. M. Blackwell, J. F. Case, S. H. D. Haddock, C. M. Herren, C. M. Orrico, and E. Terrill (2009), Bioluminescence to reveal structure and interaction of coastal planktonic communities, *Deep Sea Res. Part II*, *56*(3–5), 232–245, doi:10.1016/j.dsr2.2008.08.002.

Paduan, J. D., and I. Shulman (2004), HF radar data assimilation in the Monterey Bay area, *J. Geophys. Res.*, *109*, C07S09, doi:10.1029/2003JC001949.

Paduan, J. D., K. C. Kim, M. S. Cook, and F. P. Chavez (2006), Calibration and validation of direction-finding high frequency radar ocean surface current observations, *IEEE J. Oceanic Eng.*, *31*, 862–875, doi:10.1109/JOE.2006.886195.

Rabier, F., E. Klinker, P. Courtier, and A. Hollingsworth (1996), Sensitivity of forecast errors to initial conditions, *Q. J. R. Meteorol. Soc.*, *122*, 121–150, doi:10.1002/qj.49712252906.

Ramp, S. R., J. D. Paduan, I. Shulman, J. Kindle, F. L. Bahr, and F. Chavez (2005), Observations of upwelling and relaxation events in the northern Monterey Bay during August 2000, *J. Geophys. Res.*, *110*, C07013, doi:10.1029/2004JC002538.

Ramp, S. R., et al. (2009), The Autonomous Ocean Sensing Network (AOSN) predictive skill experiment in the Monterey Bay, *Deep Sea Res. Part II*, *56*(3–5), 8–26.

Rhodes, R. C., et al. (2002), Navy Real-Time Global Modeling Systems, *Oceanography*, *15*(1), 29–43.

Rosenfeld, L. K., F. B. Schwing, N. Garfield, and D. E. Tracy (1994), Bifurcated flow from an upwelling center: A cold water source for Monterey Bay, *Cont. Shelf Res.*, *14*, 931–964, doi:10.1016/0278-4343(94)90058-2.

Rosmond, T. E., J. Teixeira, M. Peng, T. F. Hogan, and R. Pauley (2002), Navy Operational Global Atmospheric Prediction System (NOGAPS): Forcing for ocean models, *Oceanography*, *15*, 99–108.

Sherman, J., R. E. Davis, W. B. Owens, and J. Valdes (2001), The autonomous underwater glider "Spray," *IEEE J. Oceanic Eng.*, *26*, 437–446, doi:10.1109/48.972076.

Shulman, I., D. J. McGillicuddy Jr., M. A. Moline, S. H. D. Haddock, J. C. Kindle, D. Nechaev, and M. W. Phelps (2005), Bioluminescence Intensity modeling and sampling strategy optimization, *J. Atmos. Oceanic Technol.*, *22*, 1267–1281.

Shulman, I., et al. (2007), Modeling of upwelling/relaxation events with the Navy Coastal Ocean Model, *J. Geophys. Res.*, *112*, C06023, doi:10.1029/2006JC003946.

Shulman, I., et al. (2009), Impact of glider data assimilation on the Monterey Bay model, *Deep Sea Res. Part II*, *56*(3–5), 128–138.

Spillane, M. C., D. B. Enfield, and J. S. Allen (1987), Intraseasonal oscillations in sea level along the west coast of the Americas, *J. Phys. Oceanogr.*, *17*, 313–325, doi:10.1175/1520-0485(1987)017<0313:IOISLA>2.0.CO;2.

Webb, D. C., P. J. Simonetti, and C. P. Jones (2001), SLOCUM: An underwater glider propelled by environmental energy, *IEEE J. Oceanic Eng.*, *26*, 447–452, doi:10.1109/48.972077.

Wilks, D. S. (1995), *Statistical Methods in the Atmospheric Sciences*, 467 pp., Academic, San Diego, Calif.

Winant, C. D., R. C. Beardsley, and R. E. Davis (1987), Moored wind, temperature, and current observations made during Coastal Ocean Dynamics Experiments 1 and 2 over the northern California continental shelf and upper slope, *J. Geophys. Res.*, *92*, 1569–1604, doi:10.1029/JC092iC02p01569.

S. Anderson, S. DeRada, C. Rowley, and I. Shulman, Oceanography Division, Naval Research Laboratory, Mail Code 7331, Stennis Space Center, MS 39529, USA. (igor.shulman@nrlssc.navy.mil)

J. Doyle, Marine Meteorology Division, Naval Research Laboratory, 7 Grace Hopper Ave., Mail Stop 2, Monterey, CA 93943, USA.

S. Ramp, Monterey Bay Aquarium Research Institute, 7700 Sandholdt Rd., Moss Landing, CA 95039, USA.